OPEN ACCESS
Modern Physics Letters B
Vol. 36, No. 36 (2022) 2250167 (19 pages)

DOI: 10.1142/S0217984922501676

Fractal analysis and ferroelectric properties of $Nd(Zn^{1}/_{2}Ti^{1}/_{2})O_3$(NZT)

Kouros Khamoushi*

Faculty of Engineering and Natural Science,
Tampere University, P. O. Box 1001,
FI-33014, Tampere 33720, Finland
**kouros.khamoushi@tuni.fi*

Cristina Serpa

Instituto Superior de Engenharia de Lisboa
and Centro de Matemática,
Aplicações Fundamentais e Investigação
Operacional, Portugal
mcserpa@fc.ul.pt

Received 23 February 2022
Revised 29 September 2022
Accepted 19 October 2022
Published 19 January 2023

The challenges in productivity of satellite mobile devices are growing rapidly to overcome the question of miniaturization. The intention is to supply the electrical and microwave properties of materials by discovering their outstanding electronic properties. Neodymium Zinc Titanate (NZT) can be a promising ferroelectric material due to its stable dielectric and microwave properties. The grain size and shape of NZT have a strong influence on overall material performances. Therefore, shape, reconstruction and property of the coming compound take an important part and can be predicted before being utilized in the devices. The significant of this research is to define ferroelectric properties of NZT and to characterize it by using Fractal Nature Analysis (FNA). FNA is a powerful mathematical technique that could be applied to improve the grain shape and interface reconstruction. The fractal structure is identified by its self-similarity. The self-similarity of an object means a repetition of shapes in smaller scales. A measure of this structure is computed using the Hausdorff dimension. It is for the first time in this investigation the Fractal analysis method is applied for the microwave materials microstructure reconstruction which makes this research an innovative work and

*Corresponding author.

will open the door for Curie–Weiss law fractal correction. In connection to our previous research for dielectric properties fractalization, we had some characterization and reconstruction data which include the Hausdorff dimension (HD).

Keywords: NZT; microwave materials: Fractal analysis; Hausdorff dimension; dielectric; ferroelectric; microstructure.

1. Introduction

Ferroelectrics and related materials are used in many applications, particularly concept of smart and intelligent materials as well as multifunctional purposes.[1] Research development has been dedicated to ferroelectric material particularly single-phase crystal materials in the thin film technology. Materials with perovskite structure have a regular atomic structure, variation, and changes in these regular repetitive grids like pattern is producing disorder of atomic domains in certain direction and polarization of materials in specific point.[2,3] Materials under influence of long-time temperature can be basis for diffusion which generate structural change or so-called phase transition.[4]

The phase transition creates ferroelectric properties of materials. This mechanism can be described as follows: when crystal material is under influence of temperature microstructure changes because of temperature variation and therefore the atomic arrangement of materials changes and phase transition occurs on a microscopic scale.[5] This also produces changes in Curie temperature and onset of polarization and finally microvolume changes of materials generate ferroelectric properties. The Curie temperature is the reason for production of weak or strong ferroelectric properties. The phase transition is dominating when solid solution composition becomes homogeneous. There is another method to synthesize ferroelectric materials by using a modified molecular beam epitaxy (MBE) system.[6] In the process of assessing ceramics materials and their properties, it is required to predict microstructures. This is vital for ceramic materials, for the use of size reduction and for a greater degree of assimilation. Even though the technique of material structure reconstruction is for the first time used on Neodymium Zinc Titanate (NZT) ceramics in this research, it can also apply to other ceramic materials. The reconstruction is based on the grain boundary Fractal analysis and the Richardson method. The most important part is to establish the relationship between the electronic properties of NZT and its microstructural fractal nature. The sample preparation contains cold powder and hot powder pressing creating sintering of the specimen. The fractal characterization takes a very important part from the powder phase up to the final microstructure analysis. Thus, the structures precisely affect electronic, physical, and several other properties of ceramic material. The establishment of microstructural properties is delivering a foundation for Fractal analysis of electronic material analysis. This application includes the influence of Hausdorff dimension (DH) from the microstructure grain boundary descriptions and link fractal corrections in Curie–Weiss law, for relative permittivity (ε_r) and magnetic permeability (μ_r).

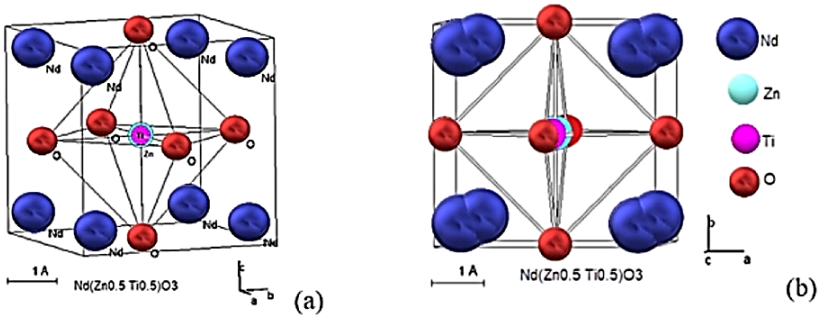

Fig. 1. (Color online) The atomic positions in NZT are shown in [100] directions (a). This model is based on monoclinic P21/n crystal structure with a lattice parameter of $a = 0.790$ nm (b). It shows a regular position of samples before keeping the sample under influence of the electrical field. The radius of Nd^{+3} is 0.127 nm, it is smaller than radius of La^{+3} (0.136 nm), therefore, it is shaken around the corner of the cube.

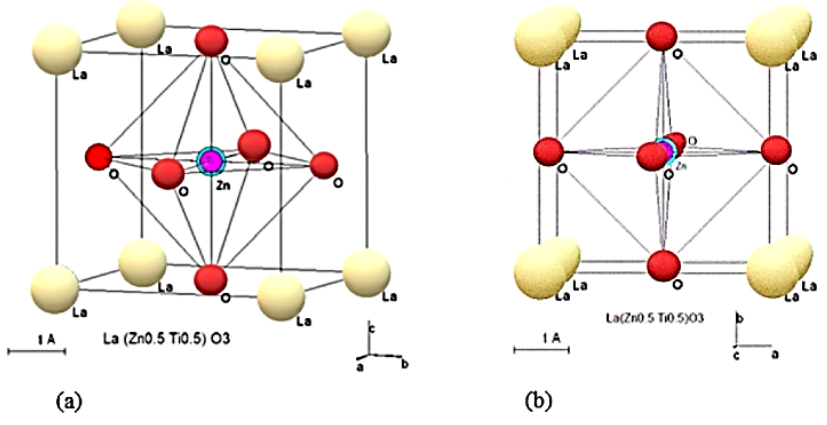

Fig. 2. (Color online) Atomic position in LZT is shown in (a) and (b). This model is based on a lattice parameter of $a = 0.790$ nm with pseudocubic crystal structure. This figure illustrates the position and location of atoms in the samples and in a standard shape. The radius of La^{+3} is equal to 0.136 nm, and it is fixed on the corner of cubic perovskite.

The previously experimental work and Neutron and Raman spectrum of neodymium zinc titanium oxide is differing noticeably from its isomorphic Lanthanum Zinc titanium oxide structure, Fig. 1 shows a model for NZT structure, these are taken from special direction to be able to investigate existing symmetry elements in packing density of atomic layers. For this model pseudo-cubic lattice parameter equal to 0.790 nm was applied.[7,8] From the point of symmetry, the general formula for complex phase is determined by $A(B'B'')X_3$, where the X refers to oxygen or other material such as fluorine in complex compounds.[9,10]

The location of Neodymium in (A) site of cube in Fig. 1 is not fixed in the position of perovskite, therefore it rattled around the corner. The Nd^{3+} with 12 coordination has a shorter atomic distance to oxygen Nd–O than La^{3+}. The Nd–O

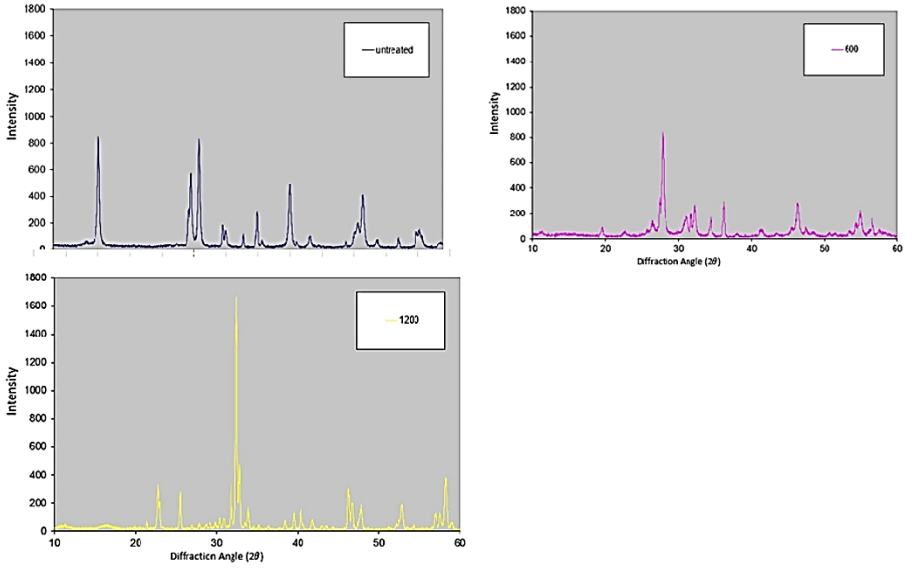

Fig. 3. (Color online) Illustrates the starting changes of Nd_2O_3 at room temperature, 600°C and 1200°C.

distance has Ionic Radius equal to $R_0 = 0.127$ nm while for La–O is $R_0 = 0.136$ nm. The atomic configuration of Lanthanum with atomic number of 57 shows different (f) electronic configuration while in Neodymium with atomic number of 60 the configuration related shows 4f,[4] the location of other atoms is similar in both conditions. The atoms in B′ and B″ condition are Zn^{2+} and Ti^{+4}, these atoms are six coordinates with the atomic radius of 0.074 nm and 0.660 nm, respectively. These distances and (f) electrical configuration result strongly on properties of materials followed by the structure changes of NZT. Therefore, NZT has a tilted monoclinic structure while Lanthanum Zinc titanium Oxide (LZT) has standard monoclinic structure.

Powder of unreacted Nd_2O_3 was evaluated by X-ray diffraction (XRD) after preparation at room temperature, 600°C and 1200°C (Fig. 3).

The original samples were tested to estimate phase evaluations at different temperatures to ensure phase variations. The hexagonal Nd_2O_3 changed to cubic Nd_2O_3 and finally reverted to hexagonal structure at 1200°C.

Based on the computer simulation and real value atomic distances and by using crystallography search match program (Crystallographica v1.60b Oxford Cryosystems Ltd.) a model based on Fig. 4 and perovskite structure was suggested for neodymium zinc titanium oxide. Perovskites are compounds with the general formula of ABX_3 where A and B are cations and X is anion, typically oxygen or fluorine. The basic ideal structure illustrated is $BaTiO_3$. Perovskite in the ideal form has cubic unit cell of complex material, the A-type atom located at the corner of

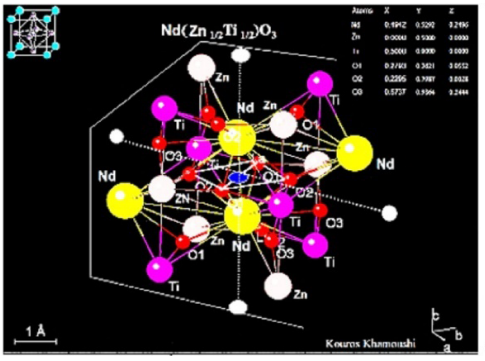

Atoms	X	Y	Z
Nd	0.4942	0.5292	0.2496
Zn	0.0000	0.5000	0.0000
Ti	0.5000	0.0000	0.0000
O1	0.2793	0.2621	0.0552
O2	0.2295	0.7978	0.0328
O3	0.5737	0.9864	0.2444

Fig. 4. (Color online) A simulation model of NZT by giving a real atomic distance to visualize in three dimensions the position of each individual atom of Nd, Ti, and Zn to be able to illustrate their real distance and link to oxygen. The Nd–O and Ti–O, Zn–O and O–O distance was calculated based on real ionic distances.

cube position (0, 0, 0), for example oxygen or fluorine, in the B sits at the body-center position (1/2, 1/2, 1/2) and oxygen atoms located at face centered positions (1/2, 1/2, 0), (1/2, 0, 1/2) and (0, 1/2, 1/2). There are also other types of perovskites where have a general formula of $A(B'B'')O_3$. The NZT material can be categorized to the later formula. The structure consists of corner linked X anion octahedra arranged in a regular fashion. Many of the materials which have similar crystal structure go through different kinds of structural phase transitions. Distortion in this kind of material can create an electrical signal for example $BaTiO_3$ can serve as a transducer.[27,28] Displacement of cations can be along a certain direction; it can be all parallel to each other in this case the crystal is defined to be a polar crystal, example of such a material is pyroelectric materials as well as piezoelectric. Otherwise, the displacements can be antiparallel leaving the crystal with a centrosymmetric structure but with a larger unit cell. The atomic distance of $BaTiO_3$ can changes by distortion or by temperature. When the temperature is above 135°C, $BaTiO_3$ has cubic structure more regular atomic distance with space group of $Pm\bar{3}m$ (O_h^1) when temperature decreases below 135°C the structure of material will change to tetragonal, this occurs by displacement of cations along one of the cube axes with respect to oxygen octahedra. The similar condition can also take place for NZT with comparable situations and distances with different critical temperatures. The distance shows the Nd located at A site and Zn and Ti at the B′ and B″ site while oxygen is placed in the corner of perovskite.

The analysis of real data with no classical geometric configuration is being a great challenge for applied science. The introduction of Fractal analysis to this kind of problem is a usual approach. We may find an extended literature performing estimates of fractal dimensions, such as box dimension (see, e.g. Refs. 35 and 36). A fractal dimension is a non-integer indicator to give a characterization of fractal

structures. The most abstract definition is the Hausdorff dimension, that is estimated by the box dimension. This is important to identify fractal irregularities on the data. A higher Hausdorff dimension means more fractal oscillations. As we may see, the properties of ferroelectric and microwave of the perovskite material system do not have characteristics compatible with the analysis of classical geometry, and a Fractal analysis makes sense to perform.

A new method of Fractal analysis is given in the literature,[34] which consists of reconstructing real data in fractal functions and is called fractal regression. These fractal functions are theoretically defined and have studied characterization, namely its estimation of Hausdorff dimension. The novelty of this method is the identification of the self-similarity of the data, not given by the measure of Hausdorff dimension itself.

Because the definition of this method is published very recently, only a few papers are using this method in the literature (see, e.g. Refs. 7, 31, 37 and 38). We will use this innovative method to analyze an unmagnetized sintered sample or pellet of NZT.

2. Experimental Procedure

To determine the ordering scale (Table 1), samples were cut and annealed at 1200°C for different lengths of time from 15 min to 105 h. The degree of ordering and the size of order domines were examined by using X-ray diffraction in NZT. The position of Zn^{+2} and Ti^{+3} located at the B-sites, as can be seen in Fig. 1, these orderings lead to an doubling of the lattice parameter of the original perovskite cell (Figs. 1 and 2), thus can be defined by X-ray diffraction spectrums. In this work, modified mixed oxide powder processing method was used. Starting powder materials include Nd_2O_3 (99.9% MELDFROM Rare Earths Ltd, UK), TiO_2 (99.8% Alfa AESAR, UK) and ZnO (99.9% ELEMENTIES Specialties, UK). In this method, the Nd_2O_3 rare earth oxide material was first purposely hydrated in distilled water to form $Nd(OH)_3$.

Table 1. Theoretical estimation based on changes in the size of order domain and ordering degree as a functioning and annealing temperature.[7]

NZT heat treatment °C	Ordered degree	Ordered domain size
No annealing	0.39	12 nm
17 min at 1100	0.49	22
35 min at 1100	0.53	32
60 min at 1100	0.61	77
3 h at 1100	0.74	95
5 h at 1100	0.86	102
7 h at 1100	0.88	102
10 h at 1100	0.91	102
26 at 1100	0.93	102
105 h at 1100	0.96	102

Fig. 5. The TEM image of NZT sample at 200 kV with camera constant of 120 which illustrates a single-phase and order of atoms.

After that stage, an amount of stoichiometric of this hydrated powder used for processing of milling in a porcelain mill pot partially filled with zirconium oxide ball and distilled water for 4 h. The 1% of Dispex A 40 (Allied Collides, Bradford, UK) mixed with powder as a deflocculant. The slurries were kept in 80°C overnight. Afterward, the powder dried and granulated with mortar and pestle and finally sieved under 250 μm. Calcination of powder occurred in two stages, first sample of powder heated to 650°C for about 2 h in an Al_2O_3 pot to ensure the dihydroxylation of $Nd(OH)_3$. To observe this stage, powder was weighed before the heating and after the heating to ensure the dihydroxylation of powder by water loss. In the second step, the powder was blended by hand and a lid placed over the pot and the powder was heated to 1200°C for 2 h again. After this step, the powder was milled again for 4 h and 2 wt.% propylene glycol (PEG 1500, Whyte Chemicals, London) being added in solution 10 min before the end. These slurries dried and finally granulated and pressed to 125 MPa in a pellet form with thickness of 3 mm and diameter of 10 mm. Sintering of NZT achieved in an alumina boat for 2 h at the temperature of 1450°C. Pellets were weighed before and after the test to calculate the degree loss of ZnO, the dense and uniform powder of NZT obtained after pressing powder by force of 125 MPa. Some sample of NZT underwent thinning by ion milling (model 600, GATAN, California, USA) for transmission electron microscope (JEM 2010, Joel, Tokyo, Japan). This sample was prepared from finished pellets for transmission electron microscope. This process involved polishing one side of pellet to 1 μm, gluing that surface onto a glass slide and grinding the pellet down to the same surface until the pellet was about 100 μm thick. After this step,

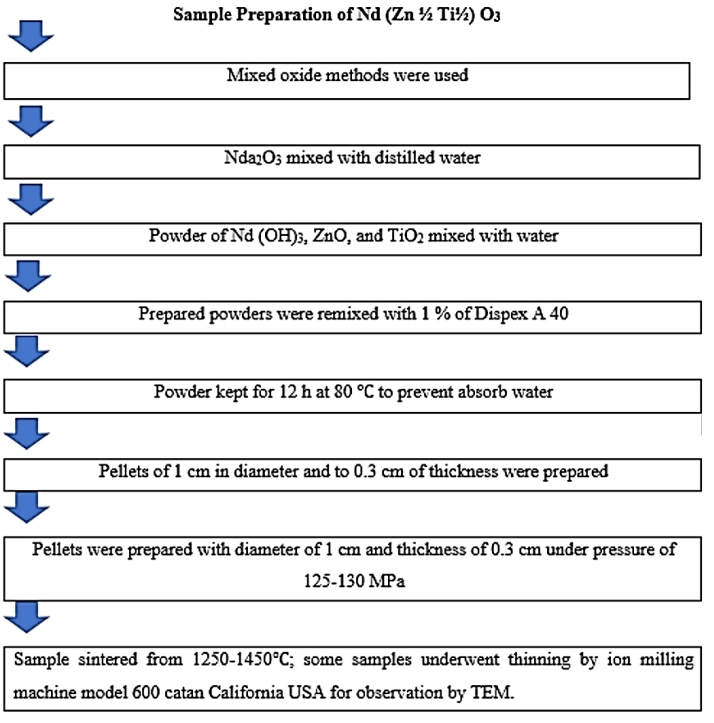

Fig. 6. (Color online) Schematic sample preparation of $Nd(Zn^1/_2Ti^1/_2)O_3$.

3mm copper ring for supporting was glued with epoxy onto the surface and allowed to set thin sample then was removed from the glass and slide on a hot plate and excess ceramics were removed from the copper rings. The remaining epoxy was dissolved in acetone. Finally, the samples were thinned to electron transparency in an ion mill.[8,11] Figure 6 shows sample preparation of NZT in brief.

The tools for testing phase evaluation and crystal structure of materials are as follows: Transmission electron microscopy (TEM), SEM, XRD, differential scanning calorimetry and rietveld method for refinement performed. The space group of specimens and phase assessment examined by the following devices: Scanning electron microscope (JSM 6300, Joel, Japan) (SEM). Siemens D5000 X-Ray Powder diffractometer.

2.1. *Ferroelectric properties of neodymium zinc titanium oxide*

A group of dielectric materials called ferroelectric materials exhibit spontaneous polarizations. One of the most used materials is barium titanate which is the most famous dielectric material. When the electric field is absent, it shows permanent magnetic behavior. The spontaneous polarization is result of the change in the positioning of Nd^{3+}, Zn^{2+}, Ti^{+4}, O^{-2} ions within the unit cell, as presented in

Fig. 1. The Nd^{+3} ions are located at the corner of unit cell which is a tetragonal and perovskite shape. The dipole moment can occur because of the displacement of O^{-2} and Ti^{4+} ions which creates a change into symmetrical shape of NZT, as can be seen in Fig. 1, the O^{2-} ions are located under the center of each face and slightly below the center of the cube.

There are many other materials which have ferroelectric properties such as Rochelle salt Potassium dihydrogen phosphate, Potassium Niobate, Lead Zirconate titanate as well as barium titanate ceramics with different materials powder size.[12,13] These materials have a relatively low frequency and extremely high dielectric constant. For example, barium titanate has very high relative permittivity of around 5000.[13] Some basic work on pure $PbTiO_3$ and many solid solutions based on those materials was carried out by other scientists such as Shirane and Takela[14] and Sawaguchi.[15]

However, recently $PbTiO_3$ ferroelectric crystal displays greater electromechanical coupling factor in comparison to their equivalents ceramic by holding the benefit of the strong anisotropy of crystals.[16] Consequently, capacitors made from these materials can be significantly smaller than capacitors made from other dielectric materials. There is a recent technology which affects these materials especially those that normally need activation energy to initiate the dipole moment and based on Curie–Weiss law to induce the magnetic moment of materials. The consequence of ion displacement accompanying the cubic tetragonal transformation can give awareness into how the spontaneous polarization could be coupled from unit cell to another unit cell.

X-ray studies have established that in tetragonal form by looking at the four central (B) Oxygen, AB′B″ ions in the cubic phase as origin. The other ions in the cube are a little shifted shown in Fig. 1 $Nd(Zn^1/_2Ti^1/_2)O_3$(NZT). It shows that if the central Ti^{4+} ion is closer to one of O^{2-} ions marked as A, it will be energetically favorite for Ti^{4+} ion on the opposite side of A to be located more distantly from O^{2+} ion in a certain area.

The similar interaction also can occur for Zn^{2+} ions. These couplings occur between neighboring columns in the NZT so that all the Ti^{4+} ions are in a stable state. If we apply an electric field the dipole moment will be in the same direction, but in some materials such as $PbZrO_3$ the ions can rotate in opposite direction in comparison to neighboring ions, so that the complete dipole moment is zero, these kinds of materials are called antiferroelectric materials.[15] The most significant property of ferroelectric ceramic materials occurs under the influence of the static electrical field when ceramic is transferred into a polar material and this activity is called poling.

The NZT ordering is related to position of Zn^{2+} and Ti^{4+} ions in B′B″ side of the perovskite crystal structure, because of the interaction between these adjacent ions the XRD indicates the broadening of position of atoms. Therefore, it creates a

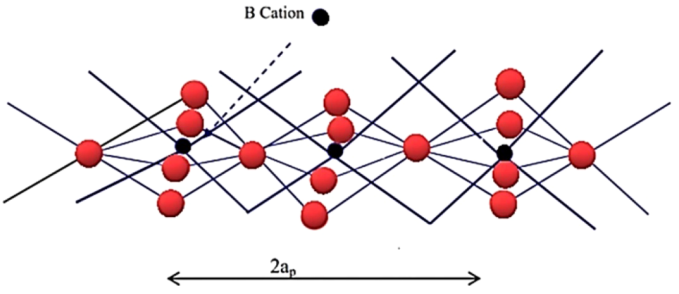

Fig. 7. (Color online) Doubling size of the NZT cube creates a superlattice by tilting the octahedra.

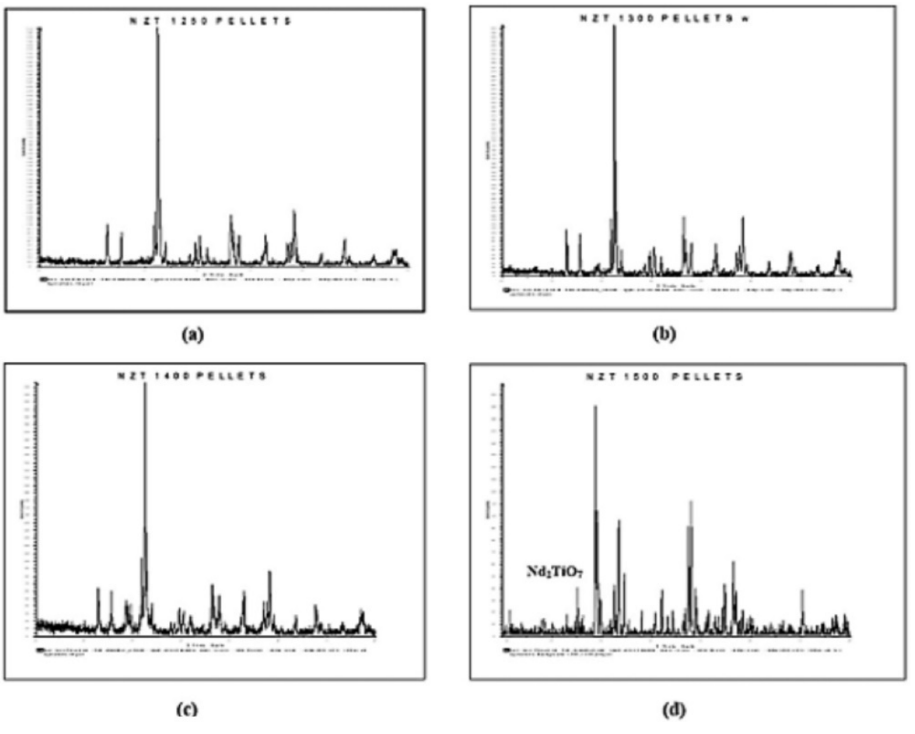

Fig. 8. XRD image of NZT samples in different temperatures.

doubling lattice distance between the A sites and B sites of atoms which are called superlattices, the result is shown in Fig. 7.

XRD series taken from 1250, 1400, 1450 and 1500°C are shown in Fig. 8, these were done by taking x-ray of each individual sample at different temperatures to determine changes and phase evaluation of samples. The specimens were identical as shown and there were no broadening and changes occurred up to temperature of 1450°C. However, as temperature increases, an unwanted phase appears at 1500°C.

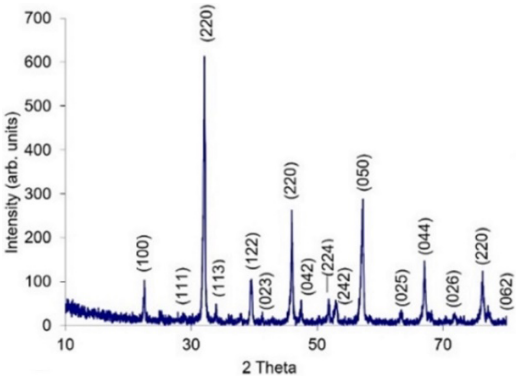

Fig. 9. (Color online) XRD of neodymium zinc titanium oxide at 1450°C.

Therefore, based on XRD evidence, the sintering temperature is identified to be 1450°C for NZT.

The vertical axes of Fig. 8 show the intensity and horizontal 2 theta angle. The angle started at 10° and ended at 80° with a stepping time of 0.6. The samples tested at room temperature of 25, 1300, 1400°C and did not show any changes as can be seen. In 1500°C, Nd_2TiO_7 appeared which was in an undesirable phase. The sample sintered at 1450°C shows an excellent perovskite crystal structure which is indexed based on 2 theta angles and checked by TEM. This sample shows a regular arrangement of atomic structure (Fig. 9).

The paper written by Pal *et al.*[17] described that Nd^{3+} substitution in $Bi_4Ti_3O_{12}$ could improve the ferroelectric properties resulting in higher remnant polarization. Field emission scanning electron micrographs (FE-SEMs) showed that the grain growth was reduced drastically with Nd^{3+} substance. The temperature and dielectric constant influenced the material behavior. When the test depolarization temperature reduces, temperature entered the maximum dielectric temperature constant (Tm) with Nd^{3+} concentration.

In the NZT, ordering locations of Zn^{2+} and Ti^{4+} ions are situated near to the B site of the cube and Nd^{3+} in the A site, these ions are spatially distributed, and it is the reason for a change in lattice parameter which leads the superlattice creation in these crystals which is shown schematically in Fig. 7. As mentioned above, the degree of changes occurring in grain boundary and remainder are based on the broadening of lattice and it is declared in Fig. 3 as starting material and could be counted based on Table 1.

These changes are strongly related to temperature and condition in how samples were treated from the starting point. As it is declared, the Nd^{3+} is hygroscopic and even absorbs water from the air which influences the crystal structure and change of the octahedral. The maximum sintering temperature for NZT is around 1450°C.

The annealing influences the change of the structure and lattice parameter. To define the ferroelectric properties of NZT, many papers such as definition and structure of different ferroelectric compounds[18] which describe the ferroelectric properties of material were used. For example, to estimate the Curie–Weiss temperature of NZT, some papers were used as follows: $Ba_{0.6}S_{0.4}TiO_3$–$La(B^1/_2Ti^1/_2)O_3$ (B = Mg, Zn) ceramics and ferrocement properties of materials[19] as well as frequency-dependent electrical properties in $Bi(Zn^1/_2Ti^1/_2)O_3$ doped $Pb(Zr_{0.4}Ti_{0.6})O_3$ and thin film for ferroelectric memory application were described by Tang *et al.*[20] Nagata and Takenaka[21] researched on $(Bi_{1/2}Na_{1/2})TiO_3$ ceramics and showed $(Bi_{1/2}Na_{1/2})TiO_3$ with Tc = 320°C, Cheuk Wai *et al.*, in paper of ferroelectric domain of the $(Bi^1/_2Na^1/_2)TiO_3$ (BNT) determined Tc to be equal to 300°C. Long *et al.* also explained perovskite structure of $(Bi^1/_2Na^1/_2)TiO_3$ (BNT) and described 320°C Curie temperature is suitable candidate when temperature is high, he described that in connection to the lead-free substances, which have a positive temperature coefficient of resistance (PTCR).[22] There was Yasuda who showed a single crystal of 24 $Pb(In^1/_2Nb^1/_2)O_3$–46 $Pb(Mg_{1/3}Nb_{2/3})O_3$–O $PbTiO_3$ by poling effect and achieved Tc = 164°C for material.[16]

Moreover, the investigation continued by research literature to be able to define the Tc of NZT, the study regarding ferroelectric and Curie–Weiss temperature is shown on Table 2, the research and more investigation shows that the NZT can have the Tc temperature around 120°C and 620°C.

The materials based on the research are described as paramagnetic material, in diamagnetic materials, atoms having no permanent magnetic dipole moments but develop dipole moments when they are under influence of an external magnetic field. Let us consider the orbiting of electrons in the atom to current loops. When an external field B_0 is employed, the fluctuation flux through the circle changes. The motion must shift so that an induced field contradicts these increases in flux. Based on Lenz' law, a calculation established on circular orbits shows that the change in

Table 2. The Curie–Weiss (TC) temperature of some materials based on Refs. 16–20.

Material name	Tc °C
$BaTiO_3$	120–130
$(Bi_{0.5}Ti_{0.5})TiO_3$	320
$BiFeO_3$	850
$Pb(In_{1/2}Nb_{1/2})O_3$–46 $Pb(Mg_{1/3}Nb_{2/3})O_3$–$PbTiO_3$	164
$Bi^1/_2Na^1/_2TiO_3$ (BNT)	300
$PbNb_2O_6$	570
$(Na^1/_2\ K^1/_2)NbO_3$	420
PZT-5A	365
$Bi_4Ti_3O_{12}$	675
$BiFeO_3$	850
$PbTiO_3$	490

movement is achieved by a slight fluctuation of orbital motion when moving upward or downward, such that the circular frequency associated ω with the orbital motion changes by

$$\Delta\omega = \pm(eB_0)/2m, \tag{1}$$

where eB_0 is the applied electric field and m is the mass of electron. The magnetic moment of electrons depends on the changes produced by the orbital frequency.[23–25]

For example, if we have a magnet and we move bismuth material near the north pole of the magnet, in this situation, the field changes and as a result it is increasing the flux through the current loop that corresponds to the distributing electron in the bismuth atom. In this situation there will be an induced field which moves in the opposite direction according to Lenz's Law. Based on this new situation, the two north poles repel one another. North pole of the magnet is induced.

The main characterization of ferromagnetic components is that they show a permanent magnetization, which suggests a natural tendency of the magnetic moment of its atoms or molecules to align under their mutual interactions. The example of ferroelectric substances is loadstone as well as natural magnets. Therefore, there are similarities between ferroelectricity and ferromagnetism with different origins. As has been described, there is an interchange between the two electrons, let's say spin S1 and S2 which is shown by $-J$S1 S2 where J is called the exchange integral, which describes the energy and distances between electrons and orbitals overlapping distribution.

The model suggested by Heisenberg is $U = -2$JSi.Sj. In the microscopic region, if J is positive and S1 and S2 are parallel, the orientations of electrons arise in the region which is called domain. This area has dimensions of order of 10^{-8} to 10^{-12} m^3 and can include from 1021 to 1017 atoms. The material can have different orientation directions; but it depends on the crystal of substance and direction of magnetization domain.[26]

The investigation of this shows that the NZT with monoclinic crystal structure and relative permittivity of 36, A site atomic number of 60 and electron configuration of [Xe] $4f^4$ $6S^2$, can have a large magnetic dipole moment because of four unpaired electrons in its electronic structure. Ferromagnetism results from having many unpair electrons in their d-block in case of Iron and its related material and f-block in the case of rare earth materials. The permittivity of NZT is calculated to be ε_NZT $= 3.186.10^{-10}$ C/Nm^2.

The coefficient of resonant frequency of this material is fluctuated around of -47 ppm/°C to -49 ppm/°C, lattice parameter $a = 0.563$ nm, $b = 0.784$ nm, and $c = 0.551$ nm with theoretical density of 6.90 g/m^3 and sintering temperature of 1450°C. Because of the high dielectric constant of NZT, this material is a suitable candidate to be used as ferroelectric material. According to electrostatic, the density of charge at the capacitor location is equal to the polarization. Electrical displacement can be calculated by the following equation:

$$D = \varepsilon_0 E + P, \tag{2}$$

where E is the electrical field P is polarization ε_0 permittivity of free space. The charge per unit area on the plate, which is the charge density (D) or electric displacement

$$D = C/V = CED = E\varepsilon_r\varepsilon_0, \tag{3}$$

C is the capacitance with the unit of Farad, the density of charge at the capacitor plate is equal to the polarization. The electrical displacement can be defined by help of Eqs. (2)–(4)

$$E = \frac{V}{d}, \tag{4}$$

where E is the electrical field, V is the voltage of two probes and (d) is the thickness of the sample or distance between the two plates. It is important to notice that D is perpendicular to the surface of the sample or plate.

3. Results and Discussions

The estimation of the calculation declared that charge density of NZT could be extremely high. We must first understand the origin and history of material. The schematic magnetic dipole moment order of the polarization of domains is illustrated in the SEM images of NZT, which are shown in Fig. 10(a) before magnetization and after magnetization in Fig. 10(b).

The investigation shows that the NZT ceramic material is a suitable candidate to achieve a high degree of ferroelectric property and can be used in the application of telecommunications and electronic devices. The comparison of NZT with several ferroelectric ceramics materials also reveals that the high dielectric permittivity and the f-block configuration of material shows the testimony of ferroelectric property. The density as well as theoretical density are significant properties of dielectric and ferroelectric materials. The slight changes such as vacancies can totally change the properties of material, therefore, a mathematical method to calculate this versatile material structure called Fractal analysis is applied.

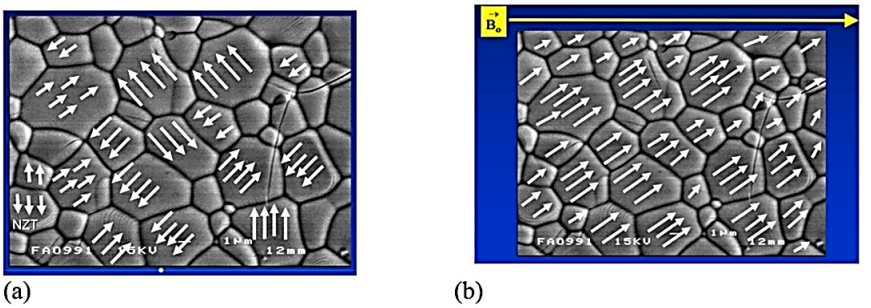

Fig. 10. (Color online) (a) Unmagnetized sample Pellet of NZT sintered at 1400°C and (b) Magnetized pellet of NZT 1400°C in direction of $B_0{}^{\rightarrow}$.

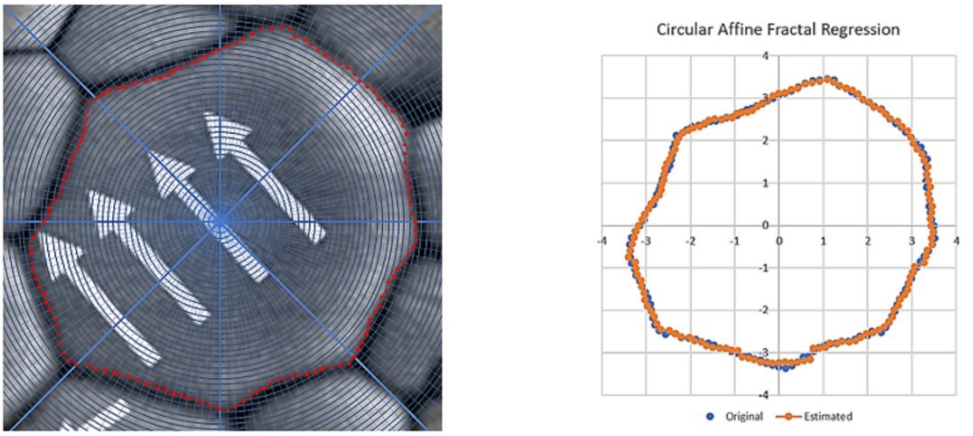

Fig. 11. (Color online) Real image and corresponding fractal reconstruction.

3.1. *Fractal analysis*

3.1.1. *Mathematical setting*

Fractal analysis is a contemporary mathematical technique that scientists use to characterize non-traditional patterns found everywhere, e.g. in nature. The most common method is the estimation of a fractal dimension. A fractal dimension is a measure of the fractal structure that generalizes the classical dimension. It is, in general, non-integer. The most used in applications is the so-called box dimension, which is estimated by splitting the global object/image into smaller box-shaped pieces and counting the number of small pieces at each scale. A more exigent theoretical definition is the Hausdorff dimension, which may be approximated by the box dimension measure.

A new approach is developed in the field of Fractal analysis, the fractal regression method. This obtains the model of a fractal function that approximates the data. Not only the fractal dimension is estimated, but also it identifies the pattern of self-similarity present in what is being studied under the form of a function. This method is based on a mathematical formulation of fractal functions given by systems of iterative functional equations. The modeled system is

$$\varphi\left(\frac{x+j}{p}\right) = a_j\varphi(x) + b_j x + c_j,$$

where $x \in [0,1)$, $0 \leq j \leq p-1$, and a_j, b_j, c_j are the parameters (real numbers) to estimate, with $0 < |a_j| < 1$. The default domain is $[0,1)$. The solution of this system is a function $\varphi : [0,1) \to \mathbb{R}$ that is called a fractal function.[29] It is proved in Ref. 32 that such functions have mathematical fractal structure. Theoretical mathematical properties and explicit solutions are provided in Refs. 30, 32 and 33. This system represents a function that is self-similar, because by definition, the image of a given

point is obtained by the image of a shifted and resized point in an affine form. In case all coefficients a_j are null, the resulted solution is a piecewise linear function.

Parameters a_j are the fractal coefficients and b_j are the directional coefficients. Bigger fractal coefficients mean strong fractal oscillations. Parameter p is the fractal period and L is the fractal level of a curve, defined by the system. The first fractal level in the entire domain will be replicated in each sub-interval (there are p sub-intervals), composing the second fractal level.

The fractal regression method consists of estimating the parameters a_j, b_j, c_j such that they fit the real data, identifying its self-similarity structure (this method is described in Ref. 34). The fitting process is done recurring to the software Fractal Real Finder.[a]

Only a few examples of this technique are studied up to now such as the nanostructures of space images from the International Space Station.[31]

With an estimated fractal curve, it is possible to upper estimate the Hausdorff dimension.[32]

Proposition. *The Hausdorff dimension of the graph of the function φ solution of the above system is upper bounded by the solution d of*

$$\sum_{j=0}^{p-1} \beta_j^d = 1,$$

$$\text{where } \beta_j = \max\left\{\frac{1}{p}, |a_j|\right\}, \quad 0 \le p \le p-1.$$

This result is obtained theoretically by studying the properties of the fractal function given by the fractal regression method. The interesting thing here is that only the fractal coefficients bigger than the inverse of the number of fractal periods are influencing the estimation of Hausdorff dimension. If all coefficients are lower than that number, then the Hausdorff dimension is equal to the classical dimension.

3.1.2. *Fractal reconstruction of data*

For the purpose of fractal reconstructing data, we take Fig. 10(a), select one piece, and consider its contour. We mark equally spaced sequential red points on this contour. These points are referenced in a polar coordinate system and form a set of radiuses corresponding to $p^L = 12^2 = 144$ angles in the contour. To perform the fractal regression, we make a change of variables from polar to Cartesian coordinates. With this data, we run the Fractal Real Finder software and obtain the estimated coefficients a_j, b_j, c_j.

[a]For information and support material, see www.researchgate.net/profile/Cristina-Serpa.

Table 3. Estimated coefficients for the fractal curve of the radius.

	0	1	2	3	4	5
a_j	−0.109	0.075	0.075	0.118	0.058	0.021
b_j	0.09	0.072	−0.797	0.319	−0.305	0.736
c_j	3.915	3.287	3.256	2.349	2.879	2.73
		7	8	9	10	11
a_j	0.073	0.089	−0.054	0.114	0.077	−0.109
b_j	0.296	−0.429	0.03	0.381	−0.169	0.052
c_j	3.102	3.185	3.39	2.595	3.099	3.771

The relevant fractal coefficients are $a_0 = -0.1086$, $a_3 = 0.1177$, $a_7 = 0.0893$, $a_9 = 0.114$ and $a_{11} = -0.1086$ (those bigger than $\frac{1}{p} = \frac{1}{12} = 0.08(3)$). The corresponding Hausdorff estimate is 1.04861. Returning to polar coordinates (radius and angle), we plot the estimated curve and compare it with the original data.

We may observed the good fitting fractal curve is obtained (See Fig. 11). The shape is analyzed in terms of a mathematical function and the given structure allows us to estimate the Hausdorff dimension, measuring the fractal nature of it.

4. Conclusions

The investigation shows that the NZT compound is a good selection to accomplish a high degree of ferroelectric property. It predominates and can be used in the application of electronic devices and electronic fields. The analogy of NZT with many other ferroelectric ceramics compounds illustrates the high dielectric permittivity and f-block configuration of material, which reveals all the testimony of ferroelectric property. The Fractal analysis shows a good fitting on the data. The fractal reconstruction done enables us to estimate the Fractal Hausdorff dimension of the contour line studies. In the Fractal analysis, the properties of microstructures are predicted. This is a fundamental purpose for miniaturization and for higher integration in electronic devices. The method of construction is used for NZT based on grain boundary Fractal analysis and Richardson methods. This research illustrates the connection between NZT ceramics materials and its electronic properties. As this is the first fractal regression application to this type of ceramic materials, more research studies would benefit by comparing results between materials and processes for obtaining materials.

Acknowledgments

Cristina Serpa acknowledges partial support from National Funding from FCT — Fundação para a Ciência e a Tecnologia, under the project: UIDB/04561/2020.

References

1. R. E. Newnham and G. R. Ruschau, *J. Am. Ceram. Soc.* **74** (1991) 463.

2. W. D. Callister, *Materials Science and Engineering, an Introduction* (John Wiley and Sons, New York, 2003), p. 390.
3. H. Yanagida, *Angew. Chem. Int.* **100** (1988) 1443.
4. A. M. Glass, *J. Appl. Phys.* **40** (1969) 4699.
5. L. Benguigui and K. Bethe, *J. Appl. Phys.* **47** (1976) 159.
6. P. S. Anderson, S. Guerin, B. E. Hayden, M. A. Khan, A. J. Bell, Y. Han, M. Pasha, K. R. Whittle and I. M. Reaney, *Appl. Phys. Lett.* **90** (2007).
7. V. V. Mitic, K. Khamoushi, C. Serpa, B. M. Randjelovic, A. Stajcic, V. Paunovic, S. Aleksic and B. Vlahovic, Fractal nature complex correction an inductivity, in *IEEE 15th International Conference on Advanced Technologies*, *Systems and Services in Telecommunications* (*TELSIKS*) (Nis, Serbia, 2021), pp. 342–347.
8. K. Khamoushi and T. Lepistö, Prediction of crystal structure and dielectric of $La(Zn^1/_2Ti^1/_2)O_3$ (LZT) and $Nd(Zn^1/_2Ti^1/_2)O_3$ (NZT), in *Properties Materials Science and Technology (Ms&T) 2006*: *Materials and Systems*, USA, Vol. 1, pp. 635–643.
9. A. M. Glazer, *Acta Crystallogr. B* **28** (1972) 3384.
10. M. Glazer and G. Burns, *Space Group for Solid State Scientists* (Academic Press, 2013).
11. K. Khamoushi, V. V. Mitic, J. Manojlović, V. Paunović and G. Lazović, *J. Mod. Phys. Lett. B* (2021).
12. L. Wu, M.-C. Chure, K.-K. Wu, W.-C. Chang, M.-J. Yang, W.-K. Liu and M.-J. Wu, *Ceram. Int.* **35** (2009) 957.
13. J. Shieh, J. H. Yeh, Y. C. Shu and J. H. Yen, *J. Mater. Sci. Eng. B* **161** (2009) 50.
14. G. Shirane and Takela, *J. Phys. Soc. J.* **7**(1) (1952) 5.
15. E. Sawaguchi, *J. Phys. Soc. J.* **8**(5) (1953) 615.
16. N. Yasuda, T. Fuwa, H. Ohwa, Y. Tachi and Y. Yamashita, The effect of poling and depoling on the dielectric and piezoelectric properties of relaxor ferroelectric solid solution single crystal of 24 $Pb(In^1/_2Nb^1/_2)O_3$–46 $Pb(Mg_{1/3}Nb_{2/3})O_3$-30 $PbTiO_3$, in *IEEE Int. Symp. Piezo Response Force Microscopy and Nanoscale Phenomena in Polar Materials* (2011), pp. 1–4.
17. V. Pal, R. K. Dwivedia and O. P. Thakur, *Mater. Res. Bull.* **51** (2014) 189.
18. J. Dai, *Ferroic Materials for Smart Systems*: *From Fundamentals to Device Applications* (Wiley - VCH Verlag Gmblt & Cuvie Weiss co. KGaA, Boschstr, 12 69469 Weinheim, Germany, 2020).
19. Y. Xu, T. Liu, Y. He and X. Yuan, *IEEE Trans. Ultrason. Ferroelectr. Freq. Control* **56**(11) (2009).
20. M. H. Tang, G. J. Dong, Y. Sugiyama and H. Ishiwara, *Semicond. Sci. Technol.* **25** (2010) 035006.
21. H. Nagata and T. Takenaka, *J. Euro. Ceram. Soc.* **11** (2001) 1299.
22. L. X. Yang, X. W. Zhu, L. Z. Li, W. Z. Jiang and X. Zhou, *Mater. Sci. Forum* **687** (2011) 411.
23. M. Alonso and E. J. Finn, *Fundamental University Physics* (Addison-Wesley Published Company, 1980).
24. F. J. Bueche, *Introduction to Physics for Scientist and Engineering* (McGraw-Hill, New York, 1980).
25. G. H. Haertling, *J. Am. Ceram. Soc.* **82** (2004) 797.
26. A. Von Hippel, *Rev. Mod. Phys.* **22** (1950).**
27. S. Yang *et al.*, *Nat. Commun.* **12** (2021) pp. 1–10.
28. W. D. Callister, Jr., *Fundamentals of Materials Science and Engineering: An Interactive e-text, Ferroelectricity* (John Wiley and Sons, New York, 2000), p. 109.
29. M. F. Barnsley, *Constr. Approx.* **2** (1986).

30. J. Buescu and C. Serpa, *J. Math. Anal. Appl.* **480** (2019) 1.
31. V. Mitić, C. Serpa, I. Ilić, M. Mohr and H.-J. Fecht, *J. Remote Sens.* **13**(9) (2021) 1.
32. C. Serpa and J. Buescu, *Constr. Approx.* **45** (2017) 273.
33. C. Serpa and J. Buescu, *Chaos Solitons Fractals* **75** (2015) 76.
34. S. Cristina, *Fractals* **30**(7) (2022), 2250138, doi:10.1142/S0218348X22501389.
35. J. Theiler, *J. Opt. Soc. Am. A* **7**(6) (1990).
36. S. Jiang and D. Liu, *Int. J. Artif. Life Res.* **3**(3) (2012) 41.
37. C. Serpa and A. Forouharfar, *Fractalization of Chaos and Complexity*: *Proposition of a New Method in the Study of Complex Systems*, Chaos, Complexity and Leadership 2020, Springer Proceedings in Complexity 2021, pp. 87–105.
38. I. M. Radovi, A. Staji, V. V. Mitic, C. Serpa, V. Paunovi and B. Randelovi, Fractal reconstruction of fiber-reinforced epoxy microstructure, in *2021 IEEE 32nd International Conference on Microelectronics* (*MIEL*) (2021), pp. 203–206, doi:10.1109/MIEL52794.2021.9569054.